ANALYSIS OF THE PLASTICITY-INDUCED FATIGUE CRACK GROWTH IN HIGH-STRENGTH STEELS

J. Toribio, V. Kharin, F.J. Ayaso,
B. González, J.C. Matos, D. Vergara and M. Lorenzo

Department of Materials Engineering, University of Salamanca
E.P.S., Campus Viriato, Avda. Requejo 33, 49022 Zamora
Tel: 980 545 000; Fax: 980 545 002, E-mail: toribio@usal.es

Abstract. This paper analyses the plasticity-induced fatigue crack growth in high-strength steels with very different yield strength, i.e., the plastic advancement of the end of a crack which is subjected to fatigue (cyclic) loading and whose tip moves (and thus the crack *does* grow) due to large geometry changes in its vicinity which promote transfer of material from the tip apex to the crack flanks, thus provoking a plastic crack growth on the basis of large plastic deformations *without* considering bond breaking or material splitting at the crack tip. Considering the cyclic loading, the *plastic* fatigue crack growth rate $(da/dN)_p$ can be obtained and a Paris-like equation such as $(da/dN)_p = C\,\Delta K^m$ may be fitted with the numerical results. Finally, an experimental validation is performed by comparing the Paris-like equation of plastic fatigue crack growth (numerically obtained) with *real* Paris equations of fatigue crack growth measured in four high-strength steels of different yield stress.

Resumen. Este artículo analiza el crecimiento de fisuras por fatiga inducido por plasticidad en aceros de alta resistencia con diferente límite elástico, es decir, el avance plástico del extremo de una fisura sometida a carga cíclica (fatiga) y cuyo extremo se mueve (y por tanto la fisura *ciertamente* crece) debido a los cambios de geometría en sus proximidades, que potencian la transferencia de material del extremo de la fisura hacia los flancos, provocando de este modo un crecimiento plástico basado en grandes deformaciones plásticas *sin* considerar la rotura de enlaces o la fragmentación de material en el extremo de la fisura. Considerando la carga cíclica, el crecimiento *plástico* de la fisura por fatiga $(da/dN)_p$ puede obtenerse mediante una ley de tipo Paris tal como $(da/dN)_p = C\,\Delta K^m$ que puede ajustarse a partir de los resultados numéricos. Finalmente, se realiza una validación experimental comparando las leyes de Paris obtenidas numéricamente con las leyes *reales* de crecimiento de fisuras por fatiga medidas en cuatro aceros de alta resistencia con distinto límite elástico.

1. INTRODUCTION

Fatigue of materials is the cause of many engineering failures, so that its understanding and characterisation in terms of controllable variables is a prerequisite for safe engineering design and maintenance. Fatigue crack growth rate *da/dN* as material's response, together with external variables governing crack propagation in a material for a particular geometry-and-loading situation, have been appreciated as the key issues in damage tolerant design [1]. Fracture mechanics concepts can be used to establish the factors controlling fatigue crack growth. In particular, when inelastic material behaviour (plasticity, damage, etc.) is localised in a small near tip domain —the small scale yielding (SSY) case— the concept of linear elastic fracture mechanics and the stress intensity factor K work well [2]. The basic relationship may be represented as:

$$\frac{da}{dN} = \mathrm{F}\,(K_{\max}, K_{\min}) = \widetilde{\mathrm{F}}\,(\Delta K, R) \qquad (1)$$

where the right hand parts are considered to be material-dependent functions, $K_{\max}$ and $K_{\min}$ are, respectively, the maximum and minimum K-values of the loading cycle; $\Delta K = K_{\max} - K_{\min}$ the stress intensity range and $R = K_{\min}/K_{\max}$ the load ratio. Ample experimental evidence favours the K-approach to fatigue cracking, and several expressions of the fatigue "law" (1) have been proposed, but none is fully capable of describing a variety of peculiarities of fatigue crack growth [1,2].

Micromechanisms of fatigue degradation and rupture are thought to be related to cyclic evolutions of stress and strain [1], whereas the K-pattern can be the controlling parameter but not a direct driver. Then analyses of fine peculiarities of local crack tip stresses and strains are essential for linking easily controllable macroscopic variables such as K with fracture mechanisms, and for characterisation and prediction of fatigue crack growth.

Numerous models have been developed to reveal the evolution of the near tip situation under cyclic loading. Some of them offered closed-form solutions, although restricted by crucial simplistic assumptions (cf. [3] and reviews in [1,2]). More realistic numerical simulations have been also performed for fatigue cracks, mostly under plane stress conditions [4-10].

This paper analyses the plasticity-induced fatigue crack growth in real high-strength steels with very different yield strength, so that the *plastic* fatigue crack growth rate can be obtained and a Paris-like equation may be fitted on the basis of the numerical results.

2. BASIC MODELLING ISSUES

The stress-strain curves of the four steels used appear in Fig. 1 and the experimental Paris laws in Fig. 2. For each particular steel, two computations were performed, the first using a perfectly plastic model (with no strain hardening and an "ideal" yield strength obtained as an average of the real yield strength and the ultimate tensile strength of the material) and the second using a strain-hardening model to reproduce the real behaviour.

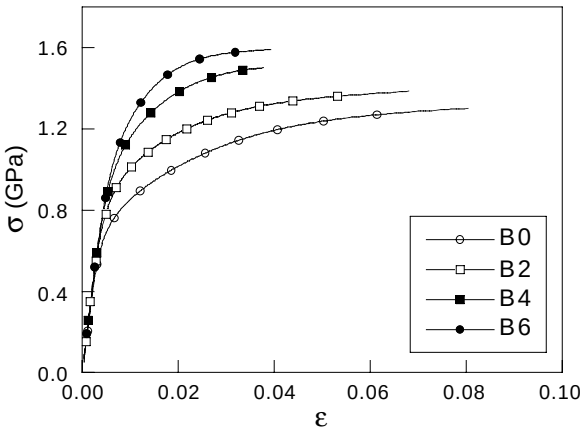

Fig. 1. Experimental σ–ε curves of the steels.

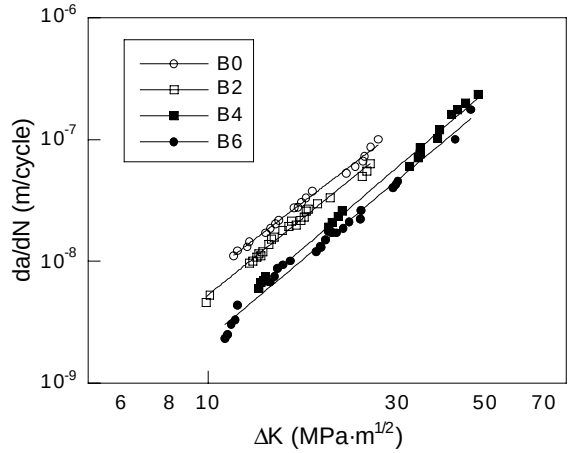

Fig. 2. Experimental Paris laws of the steels.

The crack has initially parallel flanks and smooth round-shape tip of a width (twice the tip radius) b_0, which is a good approximation [11,12]. For the considered steels the value $b_0 = 5$ μm was used [12]. The crack length was chosen adequate to enforce the conditions of *K*-dominated SSY near the tip. The double-edge-cracked panel under uniform stress σ_{app} was considered to make use of the *K*-solution from the compendium [13]. Due to symmetry, the computations were carried out for the one quarter of the panel. To avoid excessive distortion of the finite element mesh, and to allow finishing of calculations for several load reversals, the near tip mesh required more refinement than in simulations at rising-only load [11,14]. The load stepping procedure in incremental elastoplastic solution had to be finer than in reported small-strain cycling [6] and large-strain single cycle modelling [10]. Several near-tip mesh refinements were tried, and the optimum one of 1216 four-node quadrilaterals with 1292 nodes was used (Fig. 3). The solution of the boundary value problem was accomplished using the nonlinear finite element code MARC [15] with an updated Lagrangian formulation. Computations were performed using two stress intensity ranges ΔK_1 and ΔK_2 for each steel, in order to have two points of the Paris law equation (numerically predicted). The values were chosen at intermediate points of the experimental da/dN-ΔK curves shown in Fig. 2.

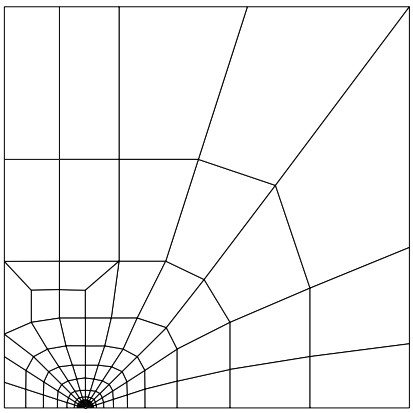

Fig. 3. Finite element mesh.

Fig. 4 shows a detail of the initial crack tip mesh where the three characteristic points A, B and C represent respectively the crack tip, the reference point for CTOD evaluation and the crack flank which allows an evaluation of crack blunting.

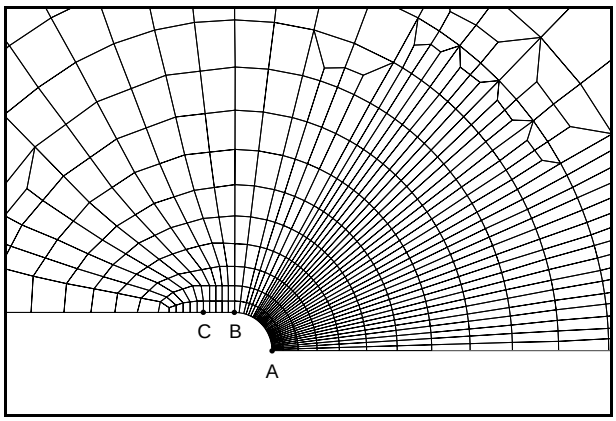

Fig. 4. Detail of the initial crack tip mesh.

3. CONVERGENCE ANALYSIS

Fig. 5 allows an analysis of the convergence of the finite element analysis by representing the crack tip displacement (key issue for obtaining the Paris law) *vs*. the number of time steps of the method for steel B4.

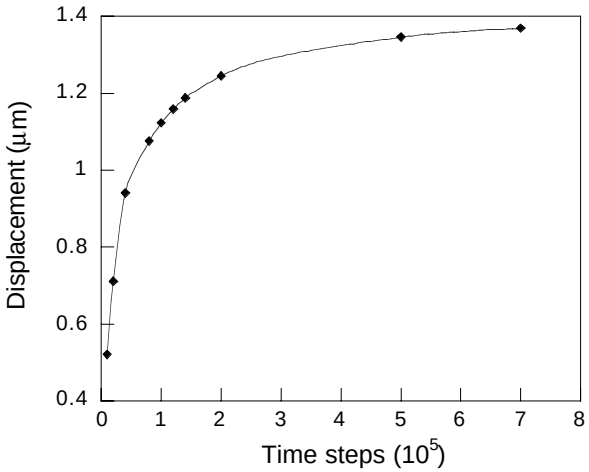

Fig. 5. Convergence curve of steel B4 (ideally plastic material model).

Fig. 6 represents the advance evolution of the crack tip during load cycles applied on steel B4, and the convergence is better as the number of time steps increases.

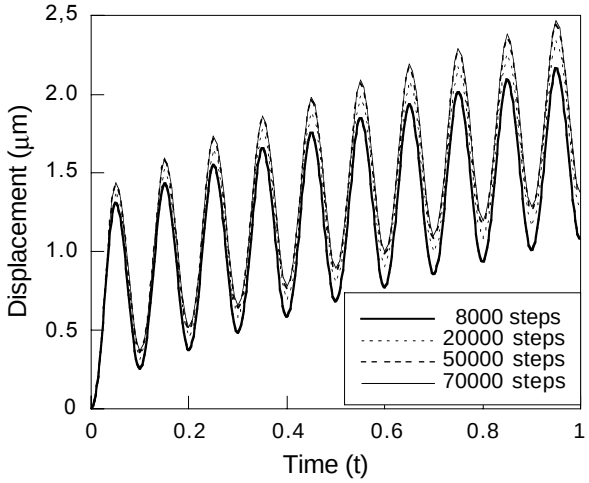

Fig. 6. Advance of the crack tip during load cycles applied on steel B4 (ideally plastic material model).

The optimum was chosen to obtain an numerical error of the crack tip displacement lower than 10%. According to this criterion, a number of 20.000 steps was considered to be adequate, as shown in the detail of Fig. 7, where results for 70.000 and 20.000 steps are really close. This time step was used in all the computations associated with the different materials, since the four stress-strain curves are similar in the matter of shape (cf. Fig. 1), although they have different size.

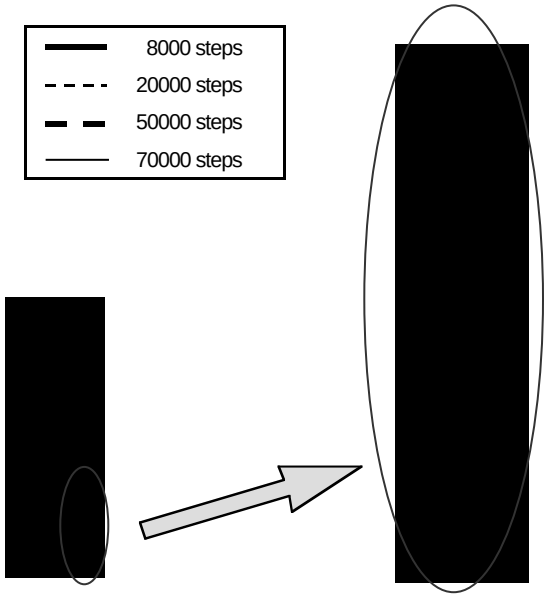

Fig. 7. Detail of the last load cycle of steel B4 (ideally plastic material model).

4. NUMERICAL RESULTS

4.1. Mesh deformation

Fig. 8 shows a detail of the deformed crack tip mesh in steel B2 at maximum load during the 10^{th} loading cycle in the case of an ideally plastic material model, whereas Fig. 9 shows the same at minimum load during the same cycle. Points A', B' and C' (Fig. 8) represent the final positions of initial points A, B and C (cf. Fig. 4) and points A'', B'' and C'' represent the same in Fig. 9. A plastic advancement of the crack tip is observed in both figures, which means that the crack *does* grow due to large geometry changes near its tip, thus promoting transfer of material from the tip apex to the crack flanks and provoking a plastic crack growth on the basis of large plastic deformations without considering bond breaking or material splitting at the crack tip.

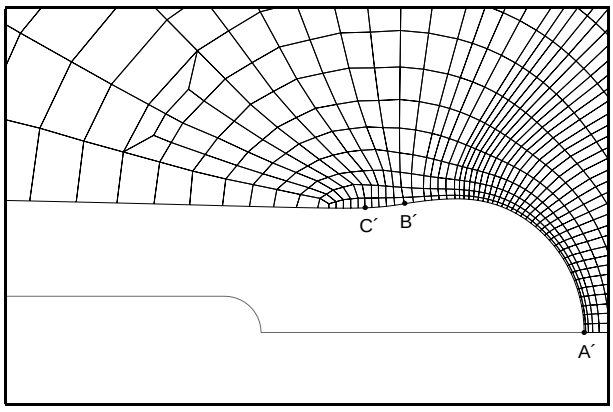

Fig. 8. Detail of the deformed crack tip mesh in steel B2 at maximum load during the 10^{th} loading cycle (ideally plastic material model). The profile of the initial crack tip shape is also shown.

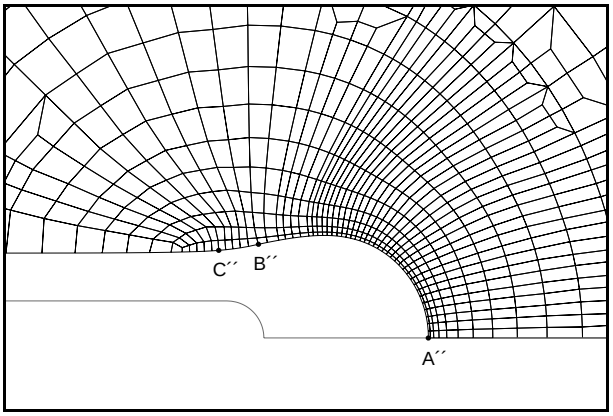

Fig. 9. Detail of the deformed crack tip mesh in steel B2 at minimum load during the 10th loading cycle (ideally plastic material model). The profile of the initial crack tip shape is also shown.

Fig. 10 shows the plastic crack tip advancement in steel B2, measured by the horizontal displacement of point A (Fig. 4). The crack length increases with time and the evolution is quasi-linear for both ΔK_1 and $\Delta K_2 > \Delta K_1$.

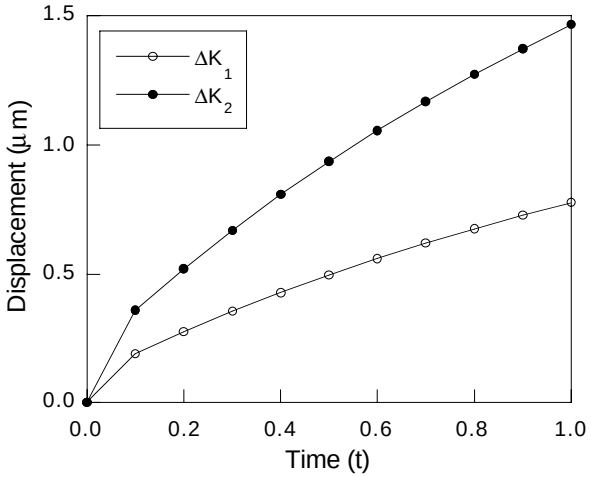

Fig. 10. Plastic crack tip advancement in steel B2 (ideally plastic material, minimum load).

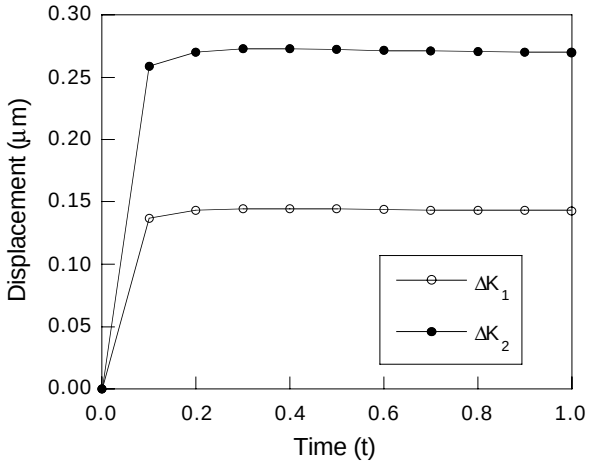

Fig. 11. Crack tip opening displacement in steel B2 (ideally plastic material, minimum load).

In Fig. 11 a plot is given of the evolution with time of the crack tip opening displacement (CTOD) measured through the vertical displacement of point B (cf. Fig. 4). The CTOD is quasi-constant during the whole loading path at the instants of minimum load (crack closing stages) of the fatigue history.

4.2. Strain evolution in the vicinity of the crack tip

Two key variables measuring the strain were considered. The first is the instantaneous equivalent plastic strain, defined as:

$$\varepsilon_{eq}^{p} = \left(\frac{2}{3} \int d\varepsilon_{ij}^{p} \int d\varepsilon_{ij}^{p} \right)^{\frac{1}{2}} \qquad (2)$$

The second is the total (cumulative) equivalent plastic strain, defined as:

$$\varepsilon_{cum}^{p} = \int d\varepsilon_{eq}^{p} \qquad (3)$$

The distributions of instantaneous and total plastic strain are shown respectively in Figs. 12 and 13 at minimum load (closing phase) during the 10th cycle, in the case of steel B2 and using an ideally plastic material model. Both figures show a strain concentration in the vicinity of the crack tip.

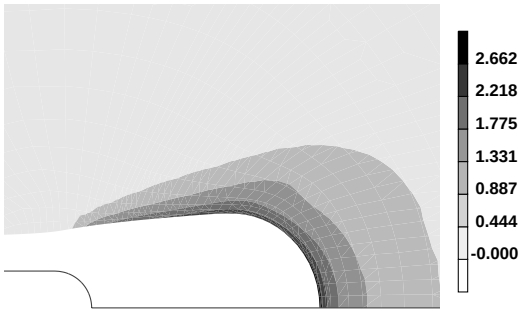

Fig. 12. Instantaneous equivalent plastic strain in steel B2, at minimum load (closing phase) during the 10th cycle (ideally plastic material model).

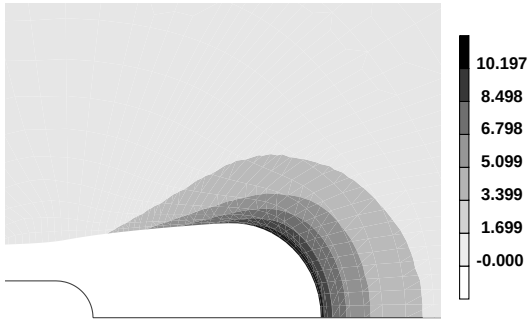

Fig. 13. Total (cumulative) equivalent plastic strain in steel B2, at minimum load (closing phase) during the 10th cycle (ideally plastic material model).

Fig. 14 gives the time evolution of both variables at the crack tip in steel B2, showing an oscillating behaviour and clear accumulation of plastic strain at the crack tip.

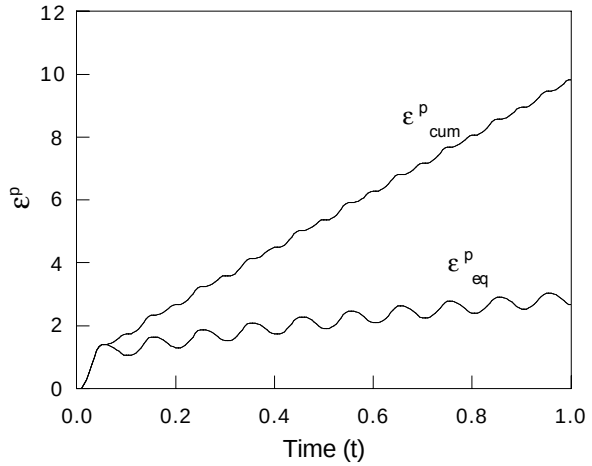

Fig. 14. Evolution with time of instantaneous and cumulative plastic strain at the crack tip in steel B2 (ideally plastic material model).

5. DISCUSSION

On the basis of the plastic crack advancement given in Figs. 8 and 9, the numerical Paris equations were obtained (Figs. 15 for an ideally plastic material model and Fig. 16 for a strain hardening material model) and compared with the real (experimental) ones (cf. Fig. 2). The strain hardening material model reproduces very well the real behaviour of the two lower strength steels (B0 and B2), but overestimates the crack growth rate in the two higher strength steels (B4 and B6), whereas the perfectly plastic material model clearly overestimates the crack growth rate in all the steels. Therefore the strain hardening models works very well, and indicates that the fatigue crack growth can be attributed to large strains and large geometry changes near of the crack tip.

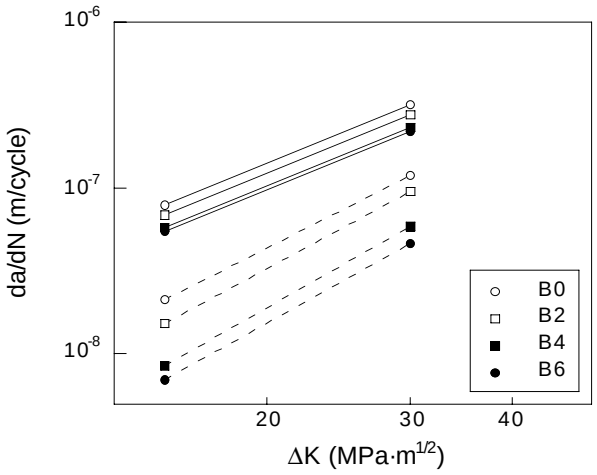

Fig. 15. Numerical (solid line) and experimental (dashed line) fatigue crack propagation laws in the case of an ideally plastic material model.

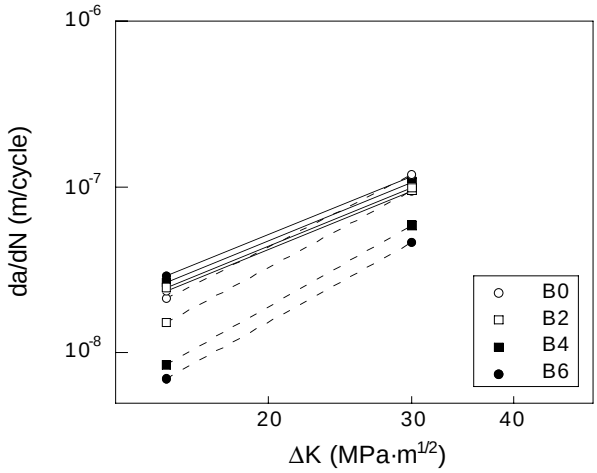

Fig. 16. Numerical (solid line) and experimental (dashed line) fatigue crack propagation laws in the case of an strain hardening material model.

With regard to the trend of crack growth rate as a function of the yield strength of the material, the ideally plastic material model reproduces the experimental trend (although the predicted magnitudes clearly overestimate the real ones, as commented in the previous paragraph), while the numerically predicted trend using the strain hardening model is opposite to the real experimental one. However, the four numerical curves in Fig. 16 are really close to each other.

Table 1 offers a summary of numerical and experimental results in the matter of the Paris constants C and m. With regard to the C constant, its variations reflect the afore said trends. In the matter of the Paris exponent m, it is seen to be quasi-constant in the numerical results, a consequence of the quasi-parallelism of the curves in both Figs. 15 and 16. A final reflection should be stated here: the numerical predictions are better for high ΔK levels and using strain hardening in the material constitutive equation.

Table 1. Values of the Paris constants in the steels.

		C (S.I.)	m
B0	Experimental	$2.51\ 10^{-11}$	2.49
	Ideally plastic	$3.52\ 10^{-10}$	2.00
	Strain hardening	$1.05\ 10^{-10}$	2.00
B2	Experimental	$1.20\ 10^{-11}$	2.64
	Ideally plastic	$3.06\ 10^{-10}$	2.00
	Strain hardening	$1.10\ 10^{-10}$	2.00
B4	Experimental	$4.43\ 10^{-12}$	2.79
	Ideally plastic	$2.54\ 10^{-10}$	2.00
	Strain hardening	$1.16\ 10^{-10}$	2.00
B6	Experimental	$4.29\ 10^{-12}$	2.73
	Ideally plastic	$2.43\ 10^{-10}$	2.00
	Strain hardening	$1.28\ 10^{-10}$	2.00

6. CONCLUSIONS

The numerical results presented in this paper allow the calculation of the plastic crack advancement caused *only* by purely plastic reasons with no account for material decohesion at the crack tip. Considering the cyclic loading, the *plastic* fatigue crack growth rate was obtained and a Paris-like equation was fitted with the numerical results. Finally, an experimental validation was performed by comparing the Paris-like equation of plastic fatigue crack growth (numerically obtained) with *real* Paris equations of fatigue crack growth in four high-strength steels of different yield stress. Numerical results demonstrated good agreement with experiments in the case of a strain hardening material model.

Acknowledgments

The financial support (Grant MAT2002-01831) of this work by the Spanish Ministry of Science and Technology (MCYT) and FEDER is gratefully acknowledged. In addition, the authors wish to express their gratitude to EMESA TREFILERIA S.A. (La Coruña, Spain) for providing the steel used in the experimental programme.

REFERENCES

[1] Suresh, S., *Fatigue of Materials*, Cambridge University Press, Cambridge (UK), 1991.

[2] Kanninen, M.F. and Popelar, C.H., *Advanced Fracture Mechanics*, Oxford University Press, New York , 1985.

[3] Rice, J.R., Mechanics of crack tip deformation and extension by fatigue, in: *Fatigue Crack Propagation, ASTM STP 415*, American Society for Testing and Materials, 1967, pp. 247-309.

[4] McClung, R.C. and Sehitoglu, H., On the finite element analysis of fatigue crack closure. —1. Basic modeling issues. —2. Numerical results. *Engng Fracture Mech*. 1989, **33**, 237-272.

[5] McClung, R.C., Crack closure and plastic zone sizes in fatigue. *Fatigue and Fract. Engng Mater. and Struct.* 1991, **14**, 455-468.

[6] McClung, R.C., Thacker, B.H. and Roy, S., Finite element visualisation of fatigue crack closure in plane stress and plane strain. *Int. J. Fracture* 1991, **50**, 27-49.

[7] Llorca, J. and Sánchez Gálvez, V., Modelling plasticity-induced fatigue crack closure. *Engng Fracture Mech*. 1990, **37**, 185-196.

[8] Ellyin, F. and Wu, J., Elastic-plastic analysis of a stationary crack under cyclic loading and effect of overload. *Int. J. Fracture* 1992, **56**, 189-208.

[9] Wu, J. and Ellyin, F., A study of fatigue crack closure by elastic-plastic finite element analysis for constant amplitude loading. *Int. J. Fracture* 1996, **82**, 43-65.

[10] Gortemaker, P.C.M., de Pater, C. and Spiering, R.M.E.J., Near-crack tip finite strain analysis, in: *Advances in Fracture Research (Proceedings of the 5th International Conference on Fracture, Cannes, 1981)*, Vol. 1, Pergamon Press, Oxford, 1981, pp. 151-160.

[11] McMeeking, R.M., Finite deformation analysis of crack tip opening in elastic-plastic materials and implications for fracture. *J. Mech. Phys. Solids* 1977, **25**, 357-381.

[12] Handerhan, K.J. and Garrison, W.M., Jr., A study of crack tip blunting and the influence of blunting behavior on the fracture toughness of ultra high strength steels. *Acta Metall. Mater.* 1992, **40**, 1337-1355.

[13] Savruk, M.P., *Stress Intensity Factors in Solids With Cracks*, Naukova Dumka, Kiev, 1988 (in Russian).

[14] McMeeking, R.M. and Parks, D.M., On criteria of *J*-dominance of crack-tip fields in large-scale yielding, in: *Elastic-Plastic Fracture*, *ASTM STP 668*, American Society for Testing and Materials, 1979, pp. 175-194.

[15] MARC User Information, Marc Analysis Research Corporation, Palo Alto, 1994.